Biophysical Journal, Volume *113*

Supplemental Information

Mapping Cell Membrane Fluctuations Reveals Their Active Regulation and Transient Heterogeneities

Arikta Biswas, Amal Alex, and Bidisha Sinha

Supplemental Information

Mapping Cell Membrane Fluctuations Reveals Their Active Regulation and Transient Heterogeneities.

Arikta Biswas, Amal Alex[#] and Bidisha Sinha[*]

Dept. of Biological Sciences, Indian Institute of Science Education and Research (IISER) Kolkata, Mohanpur - 741246, West Bengal, India

[#] Present address: Dept. of Mechanistic Cell Biology, Max Planck Institute of Molecular Physiology, 44227 Dortmund, North Rhine-Westphalia, Germany

[*] Corresponding author (email- bidisha.sinha@iiserkol.ac.in)

Table of Contents

Supporting Discussion

1. Method of calibration with beads
    a. Adherent polystyrene beads (60 µm in diameter) are imaged in the IRM mode at EM 30 and varying exposure times.
    b. Linear ROIs are drawn on the bead radially outward from the centre using ImageJ and the intensities along the lines are plotted (Fig. 1 b, *top*). Intensity vs. height plots (Fig. 1 b, *bottom*) are also plotted by converting from radial distance (x) to height (h) by

    $$h - h_0 = R - \sqrt{R^2 - x^2} \qquad \text{Eq. (1)}$$

    where, R is the radius of the bead used and h_0 is the minimum separation distance (unknown) between the bead and the substrate.
    c. From the first branch of the intensity–height profile (Fig. 1 b, *bottom*), the maximum and minimum intensity of the first branch (I_{max}, I_{min}) and the S/2 (= (I_{max}+ I_{min})/2) are plotted with the varying exposure times and fitted linearly (Fig. 1 c, *top*).
    d. The slope of the first branch is also plotted with the varying exposure times for all the line profiles (Fig. 1 c, *bottom*).
    e. Next, cells are imaged in IRM keeping exposure time fixed at 50 ms (Fig. S1 a). To obtain the cell's I_{max}, the whole cell is manually searched for pixels with high intensity values (avoiding the nucleus) (Fig. S1 a, *right*). Such maximum intensity pixels lying close (within 15 x 15 pixels) to minimas (such that when connected by a line do not cross any other maxima, Fig. S1 b) are noted down, averaged and termed as I_{max}.
    f. The cell's S/2 is calculated from the IRM images of the cell by three methods
        i. Method 1: The I_{max} and I_{min} obtained from line scans (Fig. S1 a, *right*, Fig. S1 b) are used to calculate $S/2_{method\ 1}$ ((I_{max}+I_{min}) /2).
        ii. Method 2: Large 70 x 70 pixels regions are selected inside the cell (avoiding the nucleus) (Fig. S1 a) and the mean intensity from such regions are measured as $S/2_{method2}$.
        iii. Method 3: Large 50 x 50 pixels regions are selected outside the cell (Fig. S1 a) and the mean intensity from such regions are measured as $S/2_{method3}$.

Note that the measurement/calculation of the S/2 is done in more than 20 cells in each day. It is seen that the values of S/2 calculated from the three methods are similar to each other.

Henceforth, the third method is employed for analysis since it doesn't require the actual I_{min} to be attained at any point in the cell by close attachment of the membrane to substrate.

g. The value of S/2 obtained from the cell is used to identify the exposure time at which the bead is expected to have the same value of S/2. The exposure time is noted and I_{max}, I_{min} and slope ($\Delta I/\Delta h$) of the bead at the same exposure time is read out from the respective plots (Fig. 1 c). All the three methods used for obtaining the cell's S/2 are seen to be well correlated with that of the bead (Fig. S1 c)

h. The corresponding D (= $2I_{max} - S$) is next calculated (Table S1).

i. The values of the I_{max}, S/2 and D are compared between the cell (Table S1) and the bead and is seen to be within an error of 10% from each other.

We next justify that if the bead profile has the same D, slope of intensity-height profiles of beads can indeed be used for converting ΔI to Δh in cells though their reflectivities differ.

2. Justification of method of calibration.

The interference due to the reflection off the surface of the bead can be described theoretically as (1):

$$I = I_1 + I_2 + 2\sqrt{I_1 I_2}\cos[2kh(x,y) + \phi] \qquad \text{Eq. (2)}$$

where a monochromatic incident ray I_0 is first reflected at the glass-medium interface (refractive indices, n_0 and n_1 respectively, Fig. S1 d) to give ray I_1 which is further reflected at the medium-bead interface to give rise to ray I_2 with $k = \frac{2\pi n_1}{\lambda}$ and ϕ is a phase shift usually equal to π. $h(x,y)$ is the distance between the bead and the glass substrate at lateral position (x,y), λ is the wavelength of the light used and $I_1 = r^2_{01}I_0$, $I_2 = (1-r^2_{01})r^2_{12}I_0$ with Fresnel reflection coefficient $r_{ij} = \frac{n_i - n_j}{n_i + n_j}$ (i,j = 0,1,2).

Eq. (2) can be simplified and re-written as

$$2I = S - Dcos[2kh] \quad \text{Eq. (3)}$$

where $S = I_{max} + I_{min}$ and $D = I_{max} - I_{min}$ when $I_{max} = I_1 + I_2 + 2\sqrt{I_1 I_2}$ and $I_{min} = I_1 + I_2 - 2\sqrt{I_1 I_2}$.

However, reflections from the cell membrane can be due to multiple interfaces in contrast to the bead's single interface (Fig. S1 d). In such cases, the intensity vs. height profile is expected to be described by (1):

$$2I = S - 2Dcos\{2k[h(x,y) - h_0]\} \quad \text{Eq. (4)}$$

where $h_0 = -\frac{\lambda}{4\pi n_1} arctan \frac{\gamma sin\delta}{1+\gamma sin\delta}$, with $\gamma = \frac{r_{23}}{r_{12}}(1 - r_{12}^2)$, $\delta = \frac{4\pi n_2 d}{\lambda}$ and d is the membrane thickness of index n_2.

Fig. S1 d plots both Eq. 3 (single interface) and Eq. 4 (multiple interfaces) as well as the corresponding linear fits to the central part of the first branch. As observed though the profiles do not match, the slopes are equal (single interface: 0.01182 ± 1.44E-4; multiple interface: 0.0119 ± 1.43E-4). Therefore, the using of slope of the linear part of the intensity vs. height profile from the bead for ΔI to Δh conversion for cells is justified.

However, it is also evident, and must be noted, that the bead profile cannot be used for measuring the absolute height of the cell membrane.

Since the I_{max}, S/2 and D between the cell and the bead are strongly correlated (Fig. 1 e), for the next part – identification of FBRs in the cell, I_{max} and I_{min} of the bead (imaged on the same day) are used.

3. Method of identifying FBRs
    a. Exclude minimas and maximas
        i. Using Image J, for each pixel, the minimum and maximum intensity reached in the 2048 frames captured is found out and the new images are called the minima and maxima projection respectively.
        ii. A threshold is applied on the minima projection to keep only pixels with intensities ranging from I_{min} to I_{min} + 2000. These pixels have been represented in red in Fig.1 g.
        iii. A threshold is applied on the maxima projection to keep only pixels with intensities ranging from I_{max} - 2000 to 65500. These pixels have been represented in green in Fig. 1 g.

iv. A composite image is constructed by merging the thresholded projections as represented by Fig. 1 g.

b. Manual drawing of FBRs

i. Regions close (1-pixel distance) to red pixels (avoiding the cell nucleus) are selected and square ROIs (12x12 pixels) drawn avoiding any overlap with green pixels (Fig. 1 g).

4. Justification of method to identify FBRs:

The use of minima and maxima projections ensures that a pixel is assigned to be in the first branch only if its intensity never crosses or reaches the I_{min} and I_{max} throughout the time lapse imaging. Additionally, we use the fact that if we draw a line between a red pixel and a pixel at heights above 100 nm (second branch or higher), the line would traverse intermediate heights and therefore some pixels on the line must reach intensity I_{max} of the first branch. To elaborate, a height profile of such a line on the cell is simulated (Fig. S1 f) with the height spacing between adjacent pixels as 2 nm. This is because we calculated height spacing between adjacent pixels in HeLa cells to be ~ 1.9 ± 0.6 nm (from 140 μm^2 in FBRs of a cell, as in Fig. 1 i). The bead's Intensity-Height profile (Fig. 1 b, *bottom*) next is used to read out the corresponding intensities and the resulting intensity plot shows the expected crossing through I_{max} (marked out by red arrow).

In our identification of FBRs, we hence do not include pixels which when joined to the nearest minima (red pixels) by a line pass over maximas (green pixels).

5. Check for signatures of active fluctuations in our measurements:

The following three approaches are undertaken:

A) In brief, the temporal ACFs in the FBRs of the cell frequently displayed "bumps" or "peaks". For quantifying the frequency of occurrence of these features we proceed as follows. The ACF (Figs. 2 a(vi) and 7 a, blue line) is first smoothened using Savitzky-Golay filter (Fig. 7 a, red line) and the slope or spatial derivative is calculated, smoothened and rescaled (30x fold) for visualization on the same plot (Fig. 7 a, green line).

In the absence of bumps, the slope of the ACF has a negative value which monotonically increases with time. For forming features resembling bumps or

peaks the ACF curve first flattens or the slope becomes zero (Fig. 7 a, dashed line) before further increasing. The crossing of zero (or higher threshold values (Th)) by the slope (Fig. 7 a, green line) is computed. Such crossovers located before the intersection of the ACF with the x-axis are considered to represent "bumps" or "peak". ACF curves with at least one such feature is counted and the ratio of the number of such curves over the total number of curves analyzed is computed and plotted (Fig. 7 b).

Note that increasing Th (from left to right) allows features with increasingly steeper slopes to be chosen (Fig. 7 b). As depicted in Fig. 7 b, with respect to Control cells, in ATP depleted cells the probability of finding steeper features is substantially diminished. In PMS, even lesser fraction of curves is seen to have these features. Averaging ACFs across 12x12 pixels drastically reduces the probability of finding peaks even for Control cells (Fig. 7 b). We believe this implies that the features resembling bumps/peaks may be caused by local cellular activity.

B) We next checked for the existence of any extra timescales in the ACF due to activity that are not necessarily reflected as bumps/peaks. We therefore fitted individual ACFs with a three-term multi-exponential function. Though the sharper peaks cannot be fit the baseline can be captured (Fig. 2 a(vi), solid lines). We collate the timescales and amplitudes from >1900 fits, plot the distribution of timescales weighted with their corresponding amplitudes (Fig. 3 f). On comparing the distributions among the three sets, we find that Control cells have a higher probability of having timescales ranging from 0.2-2.2 sec (Fig. 3 f, black arrow) than ATP depleted cells or PMS. This range overlaps (although having an appreciable spread) with the timescales of events of heterogeneity observed previously (Fig. 6, main text).

We believe that the smaller (<0.1sec) timescales in the distribution originate from thermal motion of the membrane and the larger (>10sec) timescales reflect the slow active/passive relaxation.

C) We also checked the effect of activity on the nature of fluctuations by analysing the height distribution at every pixel. It is reported previously (2), that activity can result in non-Gaussian nature of fluctuations. We check for the normality of the height fluctuations for every pixel using the Kolmogorov-Smirnov hypothesis testing and map the corresponding p values. We observe that the p-values vary non-uniformly across the cell. The background fluctuations are Gaussian (high p value) while

pixels inside the cell have a higher probability to be non-Gaussian (p-value < 0.05). The numbers of pixels with non-Gaussian distributions reduce on ATP depletion which when averaged over FBRs (Fig. 3 g) show significant difference from the control. Therefore, our results indicate that ATP dependent activities lead to non-Gaussian fluctuations in the cell membrane.

From these results, we conclude that the signatures of active fluctuations are very local and not evident on averaging across a length scale of 2.16x2.16 μm^2.

6. Fitting of the PSD to a model

We have fitted our PSD(f) with a model.

$$S(f) = \frac{4\eta_{eff} A k_B T}{\pi} \int_{q_{min}}^{q_{max}} \frac{dq}{(4\eta_{eff}(2\pi f))^2 + \left[\kappa q^3 + \frac{9k_B T}{16\pi\kappa}\mu q + \sigma q + \frac{\gamma}{q}\right]^2} \quad \text{Eq. (5)}$$

that is a modified version of (3) and includes the parameters –active temperature (A*T), effective viscosity (η_{eff}), bending rigidity (κ), shear modulus (μ), membrane tension (σ) and confinement (γ) as presented in Fig. 7 c. The fitting is performed using MATLAB and fits with $R^2 > 0.9$ are considered.

The PSDs used for fitting are averaged over single FBRs. It is important to note that the bumps and peaks in the ACF (Fig. 2 a(vi)) are no longer distinguishable when averaged over the whole FBR (12x12 pixels = 2.16 µm x 2.16 µm) (Fig. 7 b). We therefore feel it is justified to use the model in comparison to models where the passive thermal motion as well as contributions from active forces are considered (3). In our case the parameter A (in active temperature A*T) is used to capture the effect of activity (4). From the PSD fits, we obtained a distribution of parameter values (of A, η_{eff}, κ, μ, σ, and γ) as presented in Fig. 7 c. While other parameters fall in the expected range, the η_{eff} has values much higher (~1000 Pa-sec) than that of water or cytoplasm (0.001-0.01 Pa-sec (5)). We propose the acto-myosin cytoskeleton contributes to the η_{eff} due to the slow relaxation times of the crosslinked actin network. This is supported by the observation (Fig. 7 c) that η_{eff} reduces on perturbing the acto-myosin cytoskeleton with Cyto D or Lat B but increases by the action of Jas as well as on ATP depletion. The values of η_{eff} are also close to predictions from numerical/theoretical estimates (6).

The parameter A which indicates the degree of contribution of active motions decreases on ATP depletion (from 2.6 to 2) and on Jas treatment (from 2.3 to 1.9). The other treatments do not show in any significant change in the values of A from their respective controls. In RBCs, ATP depletion has been shown to reduce A from 3 to 1 (7).

ATP depletion in this study also leads to increase in κ, μ, σ - as observed in RBCs (3, 8). κ decreases (not significant) on Cyto D or Lat B but increases (significant) on Jas treatment. μ decreases on Cyto D and Lat B and increases on Jas treatment – though the changes are statistically not significant.

The increase in membrane tension (σ) is also seen when the cytoskeleton is perturbed by Cyto D, Lat B, or Jas. Interestingly, in RBCs too, all cytoskeletal or metabolic perturbations have been observed to lead to an increase in tension. Cytoskeleton activity and its mechanical coupling is believed to lead to softening of the membrane (3). In adherent nucleated cells, the presence of endomembrane and the cytoskeleton/ATP dependent trafficking rates need to be investigated separately in future to understand the implication of the rise in tension. Comparing the values of σ for control cells with those obtained from imaging studies (9) or tether–pulling experiments (10), we find the numbers to be in the right range (~10-450 pN/μm).

We find that the confinement parameter γ to be in the right order of magnitude (10^8-10^{10}) as predicted (4) for RBCs (10^8 J/m^4). We expect the confinement to arise from the cytoskeleton as well as connections with the ECM/ confinement due to the coverslip. We find γ to increase on ATP depletion but decrease on Cyto D, Lat B treatments. However, the γ values do not drop below 10^8 which implies the contribution of other sources. Surprisingly Jas treatments also result in reduction of γ and hence we believe that γ is not solely dependent on the presence of intact cytoskeleton.

Finally, the fits also show that the tension in mitotic cells is higher from the interphase cells as is seen in literature (11). Among the other parameters a significant increase in μ along with a significant decrease in η_{eff}, γ is seen in mitotic cells.

Table S1

Day	Cell				Bead				ΔI/Δh
	I_{min} (au)	I_{max} (au)	S/2 (au)	D (au)	I_{min} (au)	I_{max} (au)	S/2 (au)	D (au)	
1	20052 ± 2691	46461 ± 2333	33256 ± 527	26410 ± 3561	19309 ± 157	47203 ± 2147	33256 ± 1106	27895 ± 2152	320
2	20791 ± 3246	46505 ± 2090	33648 ± 694	25714 ± 4359	18960 ± 155	46335 ± 2123	32648 ± 1094	27376 ± 2129	320
3	21454 ± 2678	45407 ± 2778	33431 ± 857	23954 ± 3858	19409 ± 157	47452 ± 2153	33430 ± 1109	28044 ± 2159	320
4	12652 ± 2740	34123 ± 2201	23387 ± 912	21472 ± 3514	13196 ± 336	33576 ± 888	23386 ± 577	20381 ± 949	290
5	27175 ± 2099	45242 ± 1829	36208 ± 1263	18068 ± 2784	25498 ± 1055	46916 ± 2264	36207 ± 1599	21418 ± 2498	210
6	22326 ± 2990	42481 ± 1820	32403 ± 908	20155 ± 3500	22404 ± 243	42404 ± 901	32404 ± 493	20001 ± 933	200
7	8079 ± 1355	16665 ± 1092	12372 ± 465	8586 ± 1740	8447 ± 41	16298 ± 210	12372 ± 103	7852 ± 214	94
8	9669 ± 1042	16769 ± 801	13219 ± 312	7101 ± 1314	9125 ± 46	17312 ± 179	13219 ± 89	8188 ± 185	90
9	8128 ± 1173	15782 ± 1027	11955 ± 268	7654 ± 1559	8071 ± 106	15839 ± 553	11955 ± 303	7768 ± 563	90
10	9094 ± 15054	19709 ± 1451	14402 ± 260	10616 ± 2090	8429 ± 99	20375 ± 399	14402 ± 198	11947 ± 411	130
11	7804 ± 1263	17396 ± 1096	12600 ± 469	9593 ± 1672	7170 ± 73	18030 ± 627	12600 ± 286	10861 ± 631	100
12	6551 ± 1209	17900 ± 1267	12225 ± 362	11349 ± 1751	8025 ± 166	16425 ± 312	12225 ± 222	8400 ± 353	82
13	5779 ± 998	13130 ± 935	9455 ± 299	7352 ± 1367	6727 ± 73	12181 ± 156	9454 ± 98	5455 ± 173	80
14	13855 ± 1538	28868 ± 1629	21362 ± 462	15014 ± 2240	12481 ± 137	30246 ± 245	21363 ± 119	17765 ± 280	189
15	11983 ± 1449	28189 ± 1457	20086 ± 395	16206 ± 2055	10625 ± 71	29546 ± 210	20086 ± 110	18922 ± 221	215
16	7177 ± 1418	18173 ± 1196	12675 ± 385	10996 ± 1855	7392 ± 182	17958 ± 2032	12675 ± 1021	10566 ± 2040	108
17	5546 ± 1066	16925 ± 1012	11235 ± 157	11379 ± 1470	6620 ± 74	15850 ± 583	11235 ± 292	9230 ± 588	119
18	6562 ± 846	15216 ± 821	10889 ± 188	8654 ± 1179	5614 ± 278	16164 ± 1381	10889 ± 818	10551 ± 1408	119
19	5804 ± 1192	15549 ± 1148	10677 ± 158	9745 ±1655	5514 ± 73	15840 ± 244	10677 ± 134	10326 ± 254	116
20	6270 ±897	13838 ± 815	10054 ± 269	7569 ± 1212	5821 ± 51	14289 ± 318	10055 ± 169	8468 ± 322	102

Values of the calibration used for analysis

Values of I_{max}, I_{min}, S/2 and D for cells and beads on different days and corresponding ΔI/Δh conversions used for analysis. Details in Supporting Discussion.

Figure S1

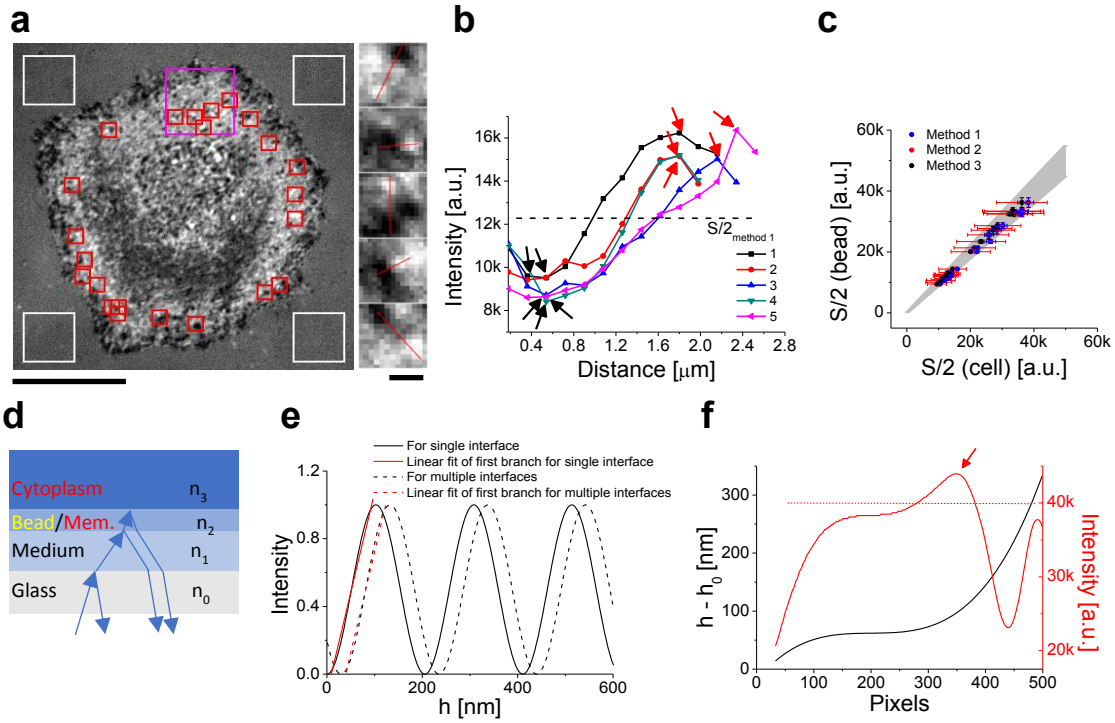

Figure S1. Justification of calibration with beads.

(a) Left: A representative IRM image of a HeLa cell with ROIs marked in red, magenta and white to calculate S/2 by methods 1, 2 and 3 (see Supporting Discussion) respectively. Scale bar: 10 μm. Right: Zoomed-in views of five FBRs with lines in red passing between minimas and maximas. Scale bar: 1 μm. (b) Profiles of lines shown in right panel of (a). Red and black arrows mark out I_{max} and I_{min} respectively and the dashed line represents $S/2_{method\ 1}$. (c) A comparison of S/2 in beads and cells (by the three methods), N = 20 days. Grey region covers $y = x \pm 0.1\ x$. (d) A schematic diagram of rays traversing through glass-medium and a single interface at the object's surface (marked as bead in yellow, relevant interfaces n_0-n_2) or multiple interfaces due to the presence of membrane as well as cytoplasm (marked in red, relevant indices n_0-n_3). (e) A comparison of simulated intensity vs. height profiles of interferences due to single and multiple interfaces with first branch fitted to a line. (f) Simulation of height and intensity for a cell with ~ 2 nm as the height spacing between two pixels. Arrow shows the I_{max} and the dotted line denotes $I_{max} - 2000$ which is used for thresholding.

Figure S2

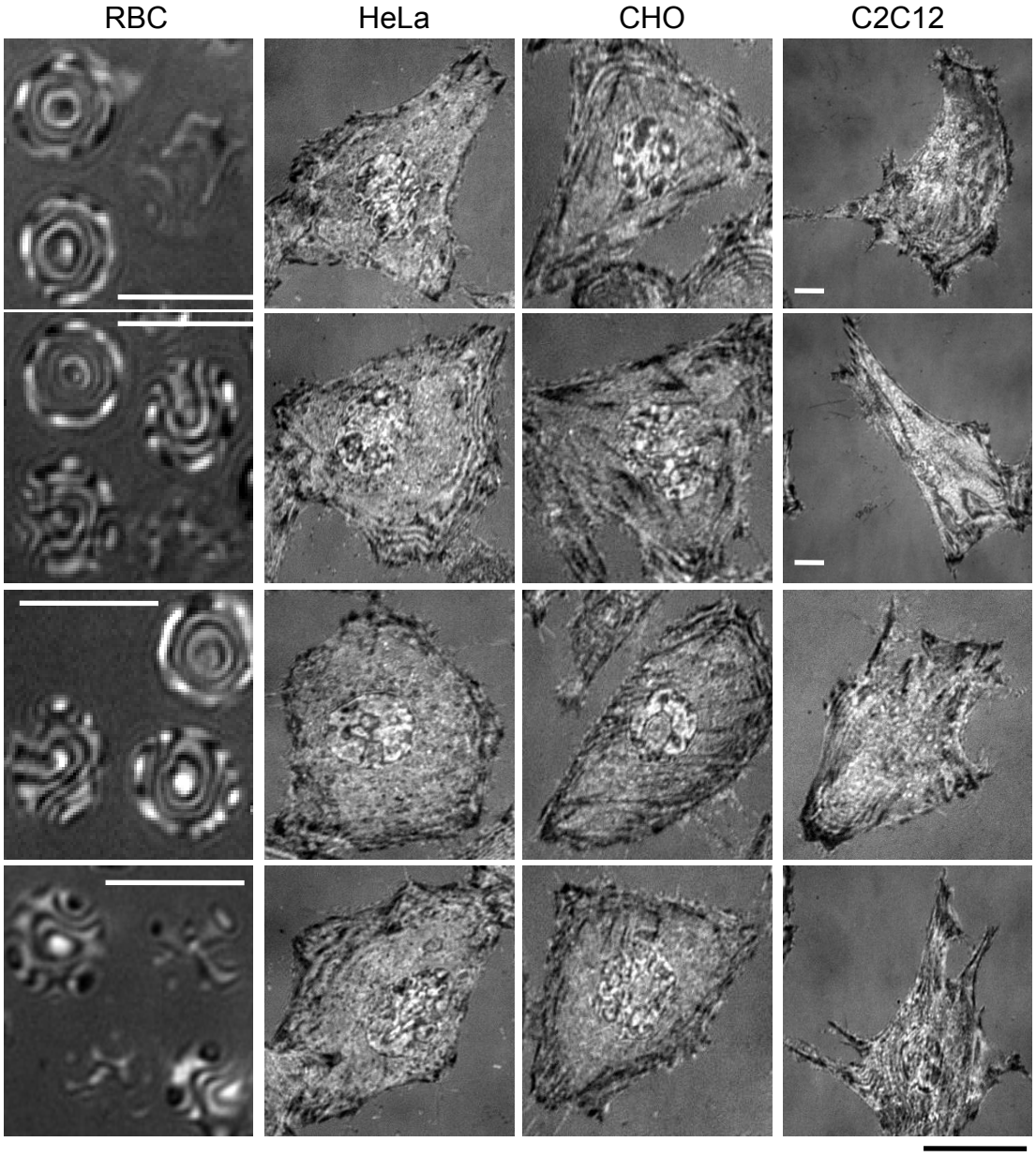

Figure S2. IRM shows heterogeneous membrane topology in cells.

Representative IRM images of adhered RBC, HeLa, CHO and C2C12 cells. Scale bar: 10 μm.

Figure S3

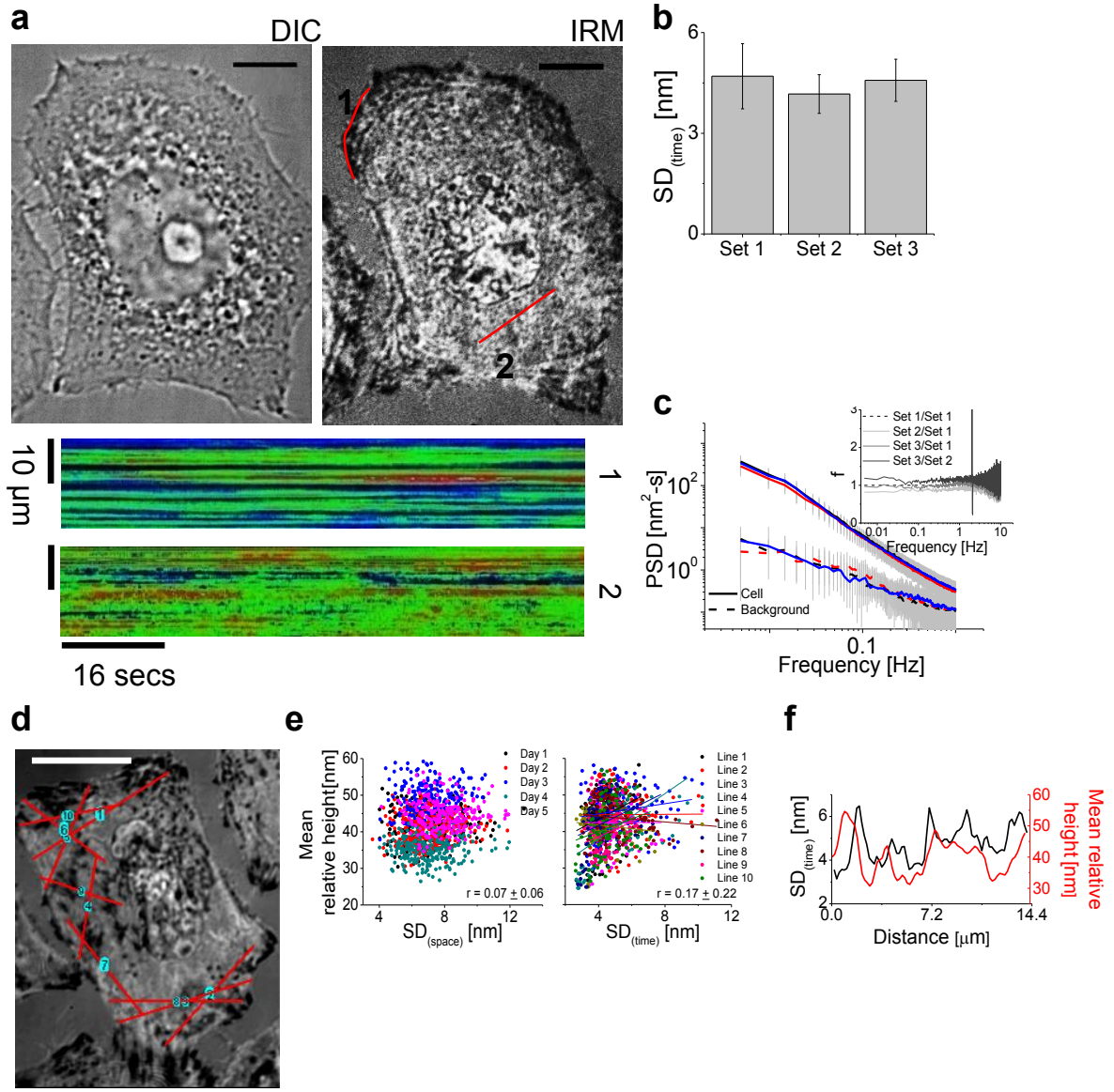

Figure S3. Temporal fluctuations and its variability.

(a) Representative images of a HeLa cell in the DIC and IRM modes (top). The temporal fluctuations across regions in a cell measured by kymographs at the marked ROIs, 1: on the focal adhesions and 2: inside the cell (bottom). (b) Temporal fluctuations across sets of experiments (N=10 cells each set) measured by $SD_{(time)}$. (c) Averaged PSDs of FBRs in cells across days and their backgrounds with inset showing *f* for the different days. (d) Line scans (red) in FBRs overlaid on a HeLa cell. Scale bar: 10 μm. (e) Plots of $SD_{(space)}$ vs. Mean relative height (left) and $SD_{(time)}$ vs. Mean relative height (right) with the average Pearson Correlation

Coefficient (r) mentioned in each. (f) The spatial profile of $SD_{(time)}$ (black) and Mean relative height (red) for two typical line scans.

Figure S4

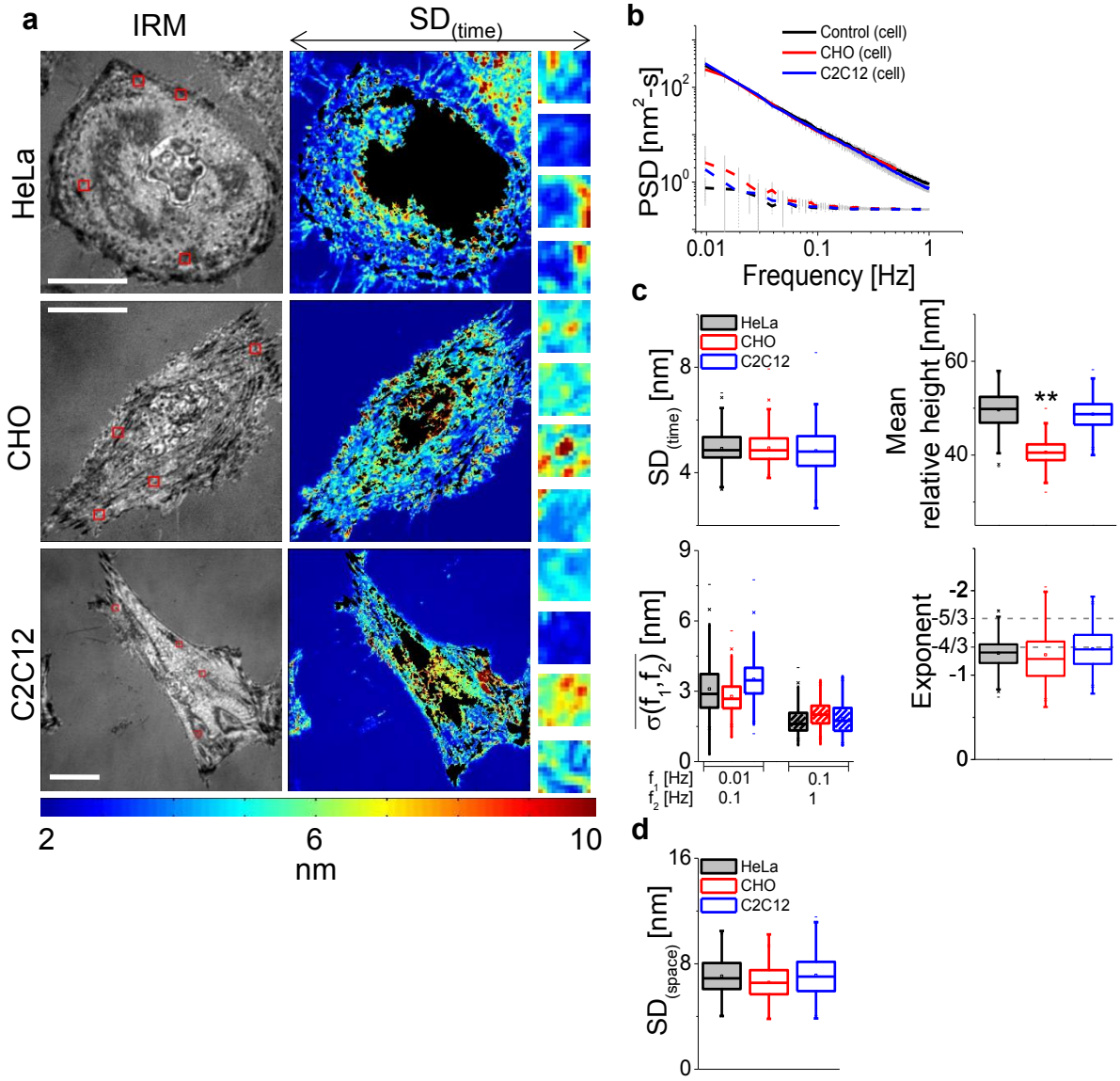

Figure S4. Similar trends of membrane fluctuations across three cell lines.

(a) IRM images (left, scale bar: 10 µm), $SD_{(time)}$ maps of the whole cells (middle, non-FBR regions blocked in black) and of four marked FBRs (right, scale bar: 1 µm) of HeLa, CHO and C2C12 cells. (b) The averaged PSDs of cells (N = 10 each, n_{HeLa} = 197 FBRs, n_{CHO} = 175 FBRs and n_{C2C12} = 219 FBRs, solid lines) and their respective backgrounds (dashed lines). (c) The

parameters of temporal fluctuations. (d) The parameters of spatial undulations. (** $p < 0.001$, One-way ANOVA). See also Table S4.

Table S2

Conditions	$\overline{\sigma(0.01Hz, 0.1Hz)}$	$\overline{\sigma(0.1Hz, 1Hz)}$	Exponent	$SD_{(time)}$	$SD_{(SD_{(time)})}$	Dissimilar pairs	$SD_{(space)}$	λ
	nm	nm		nm	nm	%	nm	nm
Control	3.0 ± 0.8	1.8 ± 0.5	-1.4 ± 0.3	5.0 ± 1.2	0.9 ± 0.3	63 ± 12	7.3 ± 1.7	505.5 ± 284.9
ATP dep.	2.1 ± 1.0	1.2 ± 0.4	-0.9 ± 0.2	3.9 ± 1.0	0.6 ± 0.4	59 ± 17	7.7 ± 2.3	478.0 ± 279.4
Cyto D	3.2 ± 0.8	2.4 ± 0.5	-1.3 ± 0.2	5.5 ± 0.8	1.1 ± 0.3	66 ± 14	7.9 ± 1.3	443.1 ± 173.7
Lat B	3.4 ± 0.8	2.5 ± 0.5	-1.3 ± 0.2	5.9 ± 0.8	1.1 ± 0.3	62 ± 13	7.9 ± 1.5	433.9 ± 183.0
Jas	2.9 ± 0.7	2.0 ± 0.4	-1.1 ± 0.2	4.3 ± 0.6	0.8 ± 0.3	65 ± 11	8.9 ± 1.5	450.6 ± 230.5
Blebb. (5 µM)	3.0 ± 0.7	1.7 ± 0.4	-1.3 ± 0.2	5.1 ± 0.7	0.9± 0.3	62 ± 8	7.9 ± 1.4	-
Blebb. (100 µM)	3.1 ± 0.9	1.7 ± 0.5	-1.3 ± 0.2	5.1 ± 0.9	1.1 ± 0.3	64 ± 10	7.9 ± 1.4	497.9 ± 240.4
Mitosis	2.3 ± 1.1	2.0 ± 0.5	-0.9 ± 0.9	4.8 ± 0.8	0.8 ± 0.3	67 ± 15	5.6 ± 2.2	418.2 ± 135.3

Parameters of temporal fluctuations and spatial undulations of HeLa cells under different conditions.

Cells highlighted in light and deep blue denote a significant decrease from the control with p-value < 0.05 and p-value < 0.001 respectively. Cells highlighted in yellow and red denote a significant increase from the control with p-value < 0.05 and p-value < 0.001 respectively. Parameters having values with no significant difference to the control are not highlighted. Mann-Whitney U test is done only on values of λ. For all the other parameters, a one-way ANOVA is done.

Figure S5

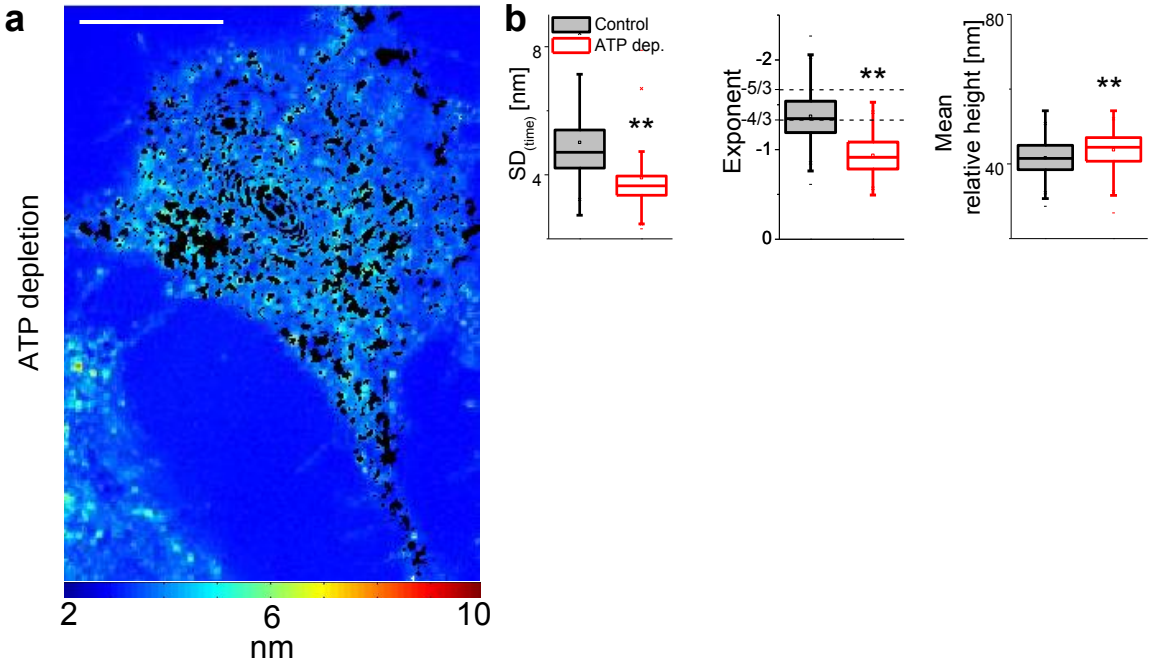

Figure S5. Detailed parameters of the effect of ATP driven processes on membrane fluctuations.

(a) Representative whole cell $SD_{(time)}$ map (non-FBR regions blocked in black) of an ATP depleted HeLa cell. Scale bar: 20 µm. (b) The parameters of temporal fluctuations ($SD_{(time)}$, Exponent and Mean relative height) in the two conditions (N = 30 cells each, $n_{control}$ = 854 FBRs, n_{ATPdep}= 964 FBRs). Asterisks indicate a significant difference (** $p<0.001$, one-way ANOVA). See also Tables S2 and S4.

Figure S6

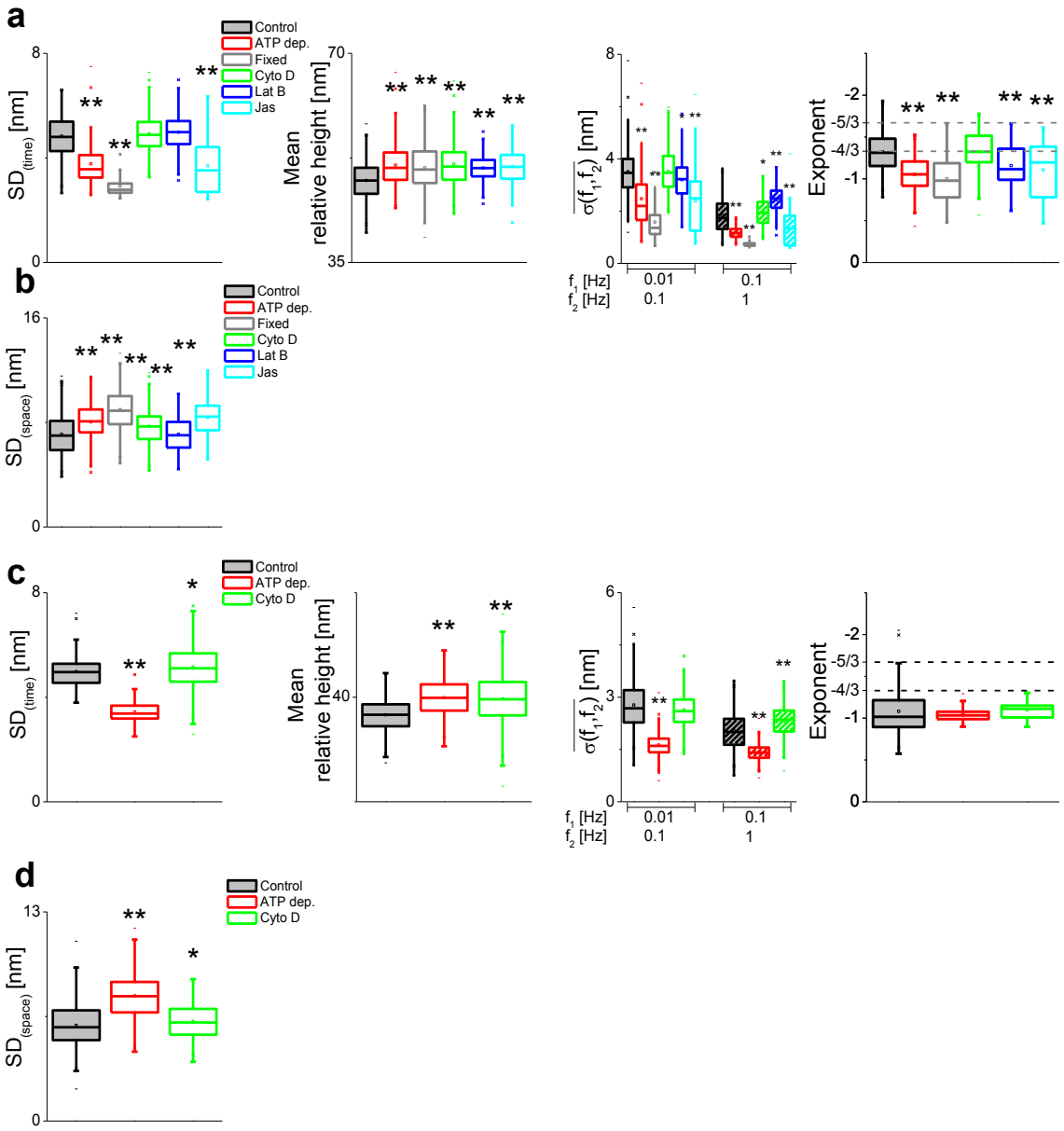

Figure S6. Detailed parameters of the behavior of cell lines under different conditions.

(a) The parameters of temporal fluctuations and (b) parameters of spatial undulations in C2C12 cells. (N = 10 cells each, $n_{control}$ = 219 FBRs, $n_{ATPdep.}$ = 139 FBRs, n_{fixed} = 171 FBRs, n_{CytoD} = 176 FBRs, n_{LatB} = 79 FBRs and n_{Jas} = 120 FBRs). (c) The parameters of temporal fluctuations and (d) parameters of spatial undulations in CHO cells. (N = 10 cells each, $n_{control}$ = 143 FBRs, $n_{ATPdep.}$ = 161 FBRs and n_{CytoD} = 137 FBRs). See also Table S4.

Figure S7

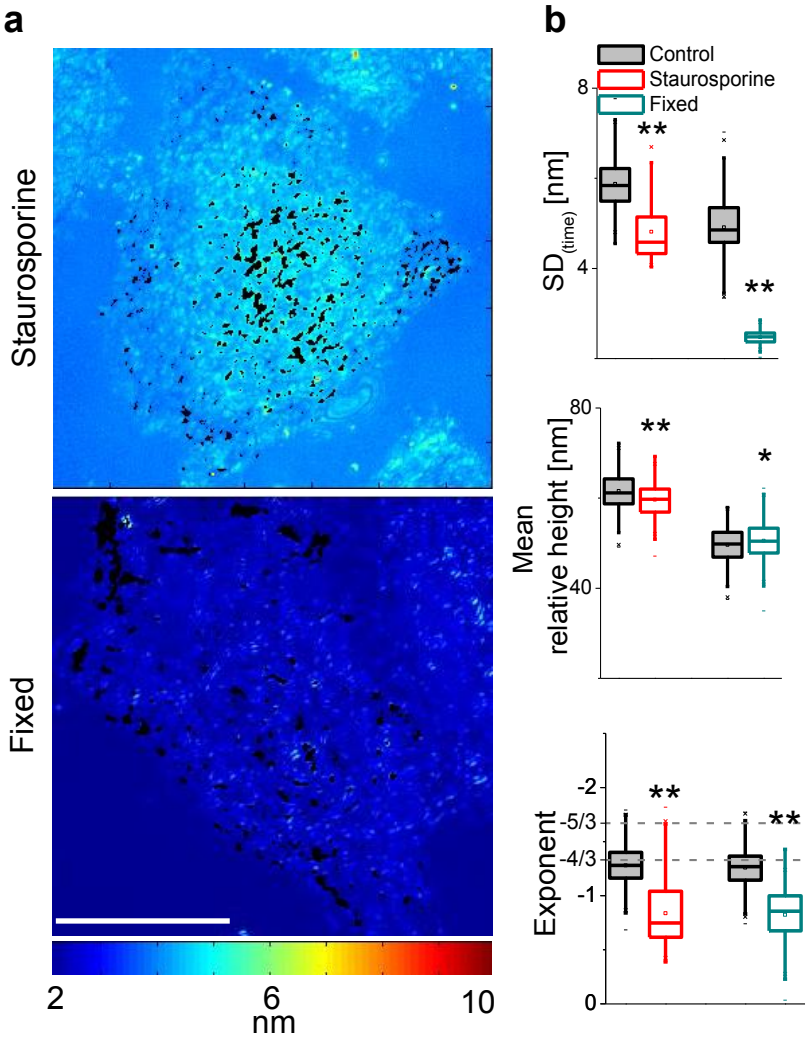

Figure S7. Detailed parameters capturing the effect of stopping cellular activity.

(a) Representative $SD_{(time)}$ maps (non-FBR regions blocked in black) of whole cells after Staurosporine treatment (left panel) and fixation (right panel). Scale bar: 10 µm. (b) The parameters of temporal fluctuations ($SD_{(time)}$, Mean relative height and Exponent) in the three conditions (N = 10 cells each, $n_{control}$ = 411 FBRs, $n_{staurosporine}$ = 310 FBRs and n_{fixed} = 331 FBRs). Asterisks indicate a significant difference (* $p < 0.05$, ** $p < 0.001$, One-way ANOVA). See also Tables S2 and S4.

Figure S8

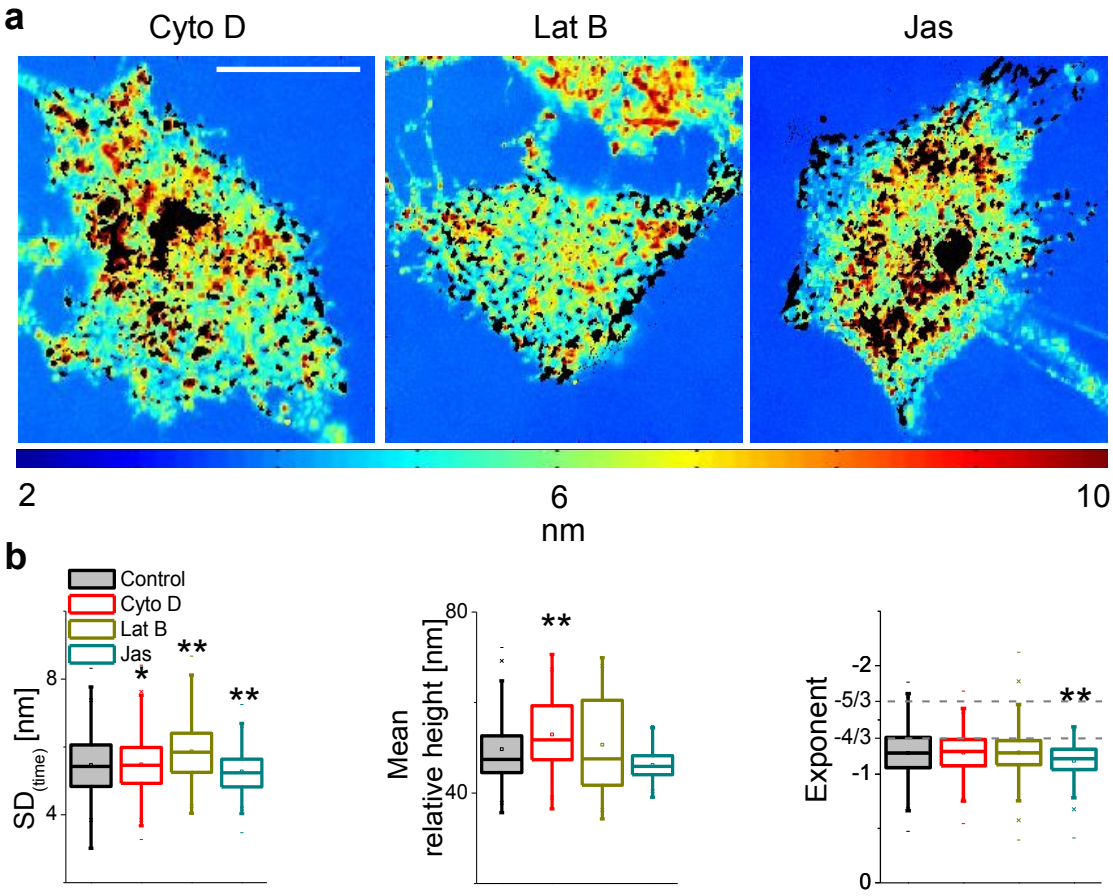

Figure S8. Detailed parameters on the effect of the cortex on membrane fluctuations.

(a) Representative $SD_{(time)}$ maps (non-FBR regions blocked in black) of a whole cell for Cyto D (left), Lat B (middle) and Jas (right) treated cells. Scale bar: 10 µm. (b) The parameters of temporal fluctuations ($SD_{(time)}$, Mean relative height and Exponent) in the different conditions (N = 30 each, $n_{control}$ = 770 FBRs, $n_{Cyto\ D}$ = 509 FBRs, $n_{Lat\ B}$ = 484 FBRs and n_{Jas} = 255 FBRs). Asterisks indicate a significant difference (* $p < 0.05$, ** $p < 0.001$, One-way ANOVA). See also Tables S2 and S4.

Figure S9

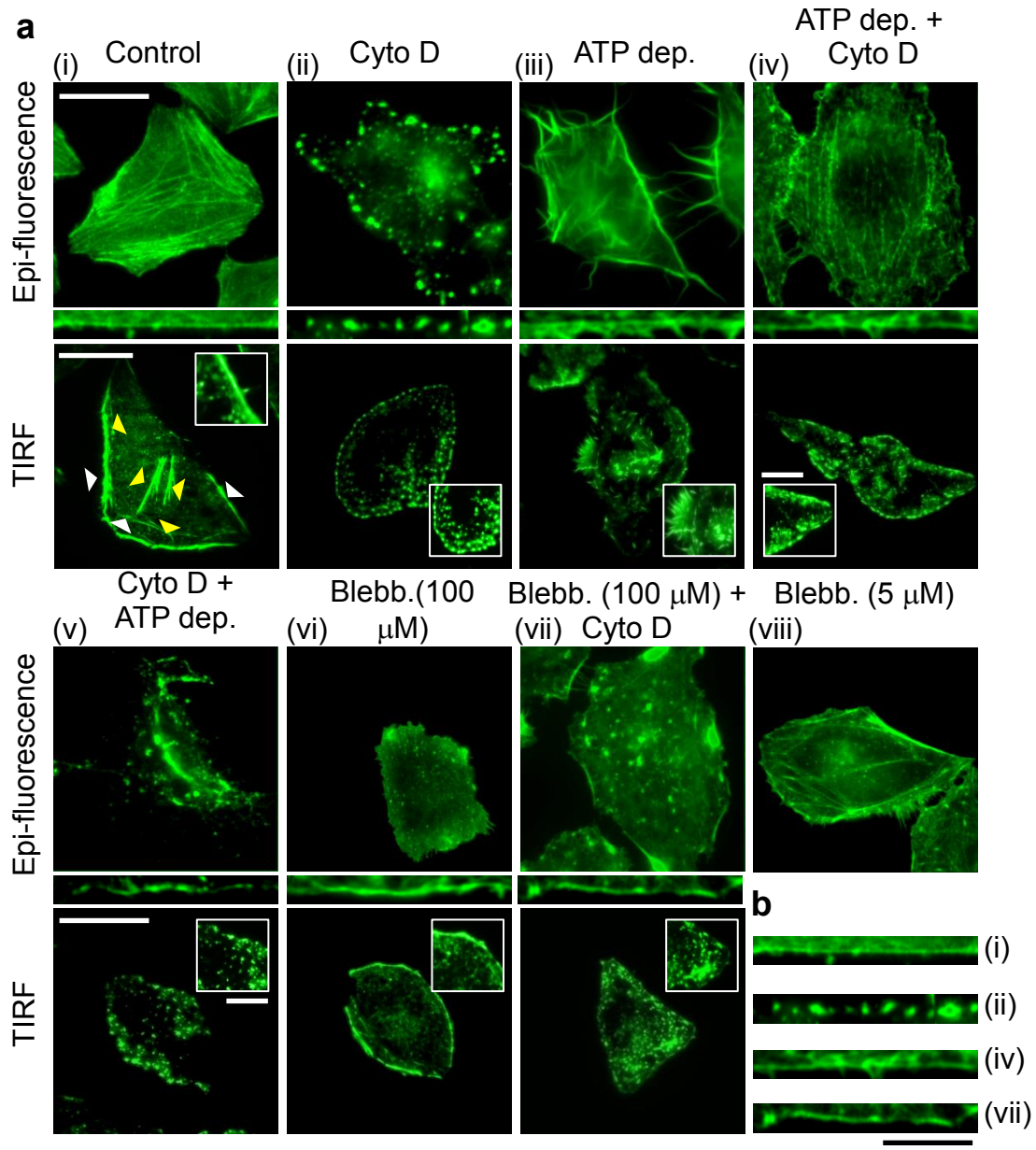

Figure S9. Quantification of cortical actin present under different conditions.

(a) Representative images of Alexa Fluor 488 Phalloidin stained cells captured in the Epi-fluorescence and TIRF (penetration depth 100 nm) modes in all the conditions (zoomed-in view in the inset, scale bar: 1 μm) along with linearized images of the cortical actin (middle) from the epi-fluorescent images. Scale bar: 10 μm. White arrowheads mark out the cortex at the edge while the yellow ones represent the stress fibres. (b) Representative images of the straightened cortex which show that pre-treatments stop cortex clearance on addition of Cyto D. Scale bar: 10 μm.

Figure S10

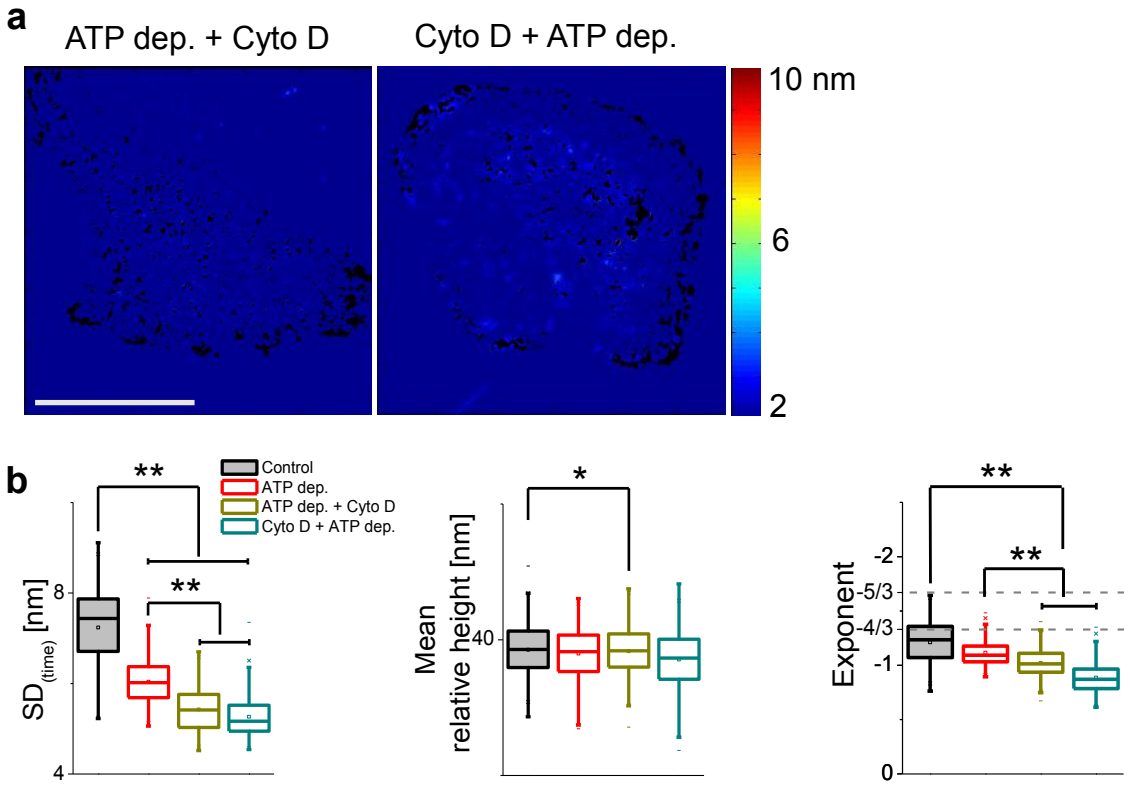

Figure S10. Detailed parameters towards the effect of polymerization while the Cyto D induced cortex clearance is blocked by ATP depletion.

(a) Representative $SD_{(time)}$ maps (non-FBR regions blocked in black) of a whole cell for ATP dep. + Cyto D treated (left) and Cyto D treated + ATP dep. (right) cells. Scale bar: 10 µm. (b) The parameters of temporal fluctuations ($SD_{(time)}$, Mean relative height and Exponent) in the different conditions (N = 10 each, $n_{control}$ = 119 FBRs, $n_{ATPdep.}$ = 158 FBRs, $n_{ATPdep.+Cyto\ D}$ = 254 FBRs and $n_{Cyto\ D+ATPdep.}$ = 162 FBRs). Asterisks indicate a significant difference (* $p < 0.05$, ** $p < 0.001$, One-way ANOVA). See also **Tables S2 and S4**.

Figure S11

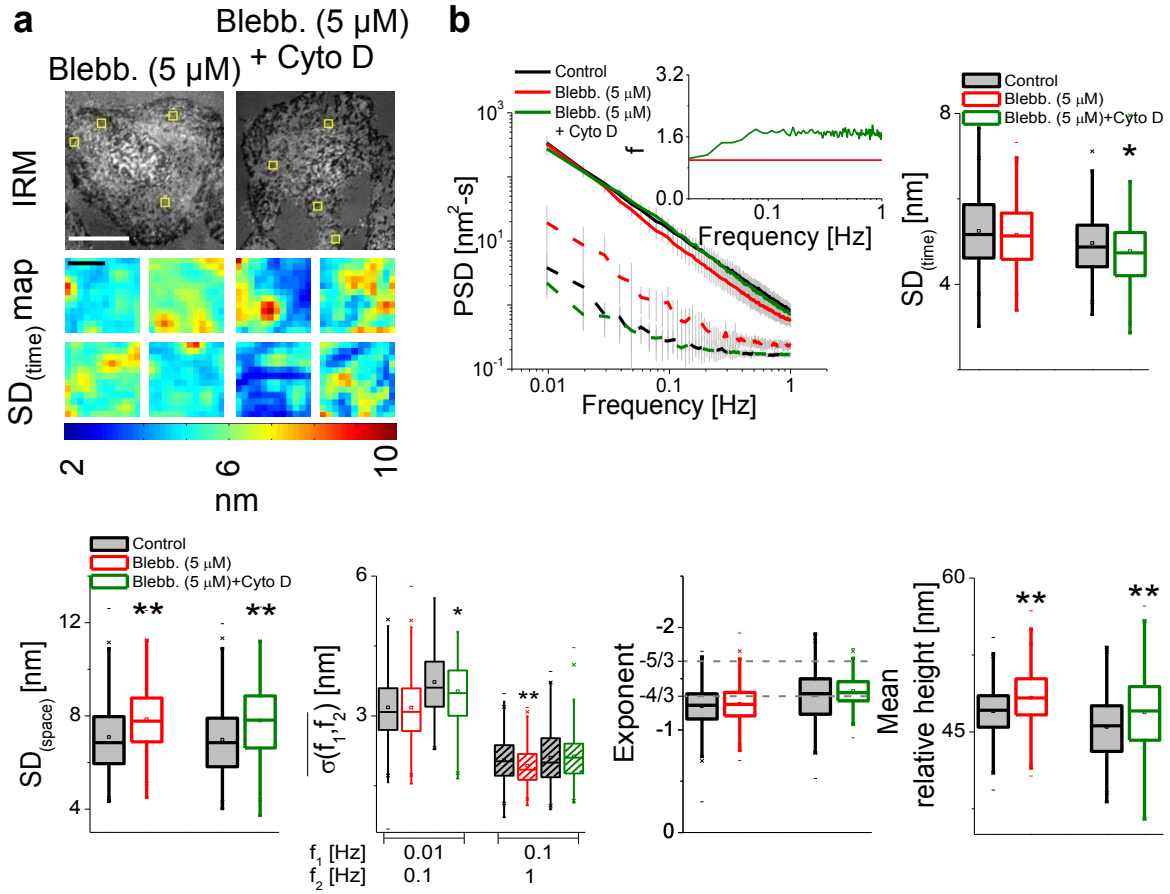

Figure S11. Low concentration of Blebb. affects fluctuations and does not stop cortex clearance by Cyto D.

(a) Representative IRM images (top, scale bar: 10 µm) and $SD_{(time)}$ maps (non-FBR regions blocked in black) of FBRs (bottom, scale bar: 1 µm) of control, Blebb. (5 µM), Cyto D after Blebb (5 µM) treated HeLa cells. (b) The averaged PSDs of cells (N = 10 each, $n_{control}$ = 175 FBRs, $n_{Blebb.}$ = 190 FBRs and $n_{Blebb.+CytoD}$ = 90 FBRs, solid lines) and their respective backgrounds (dashed lines); *f* in inset (Blebb. (5 µM) used as control for this measurement) with the parameters of spatio-temporal fluctuations. Asterisks indicate a significant difference (* $p < 0.05$, ** $p < 0.001$, One-way ANOVA). See also **Tables S2 and S4**.

Figure S12

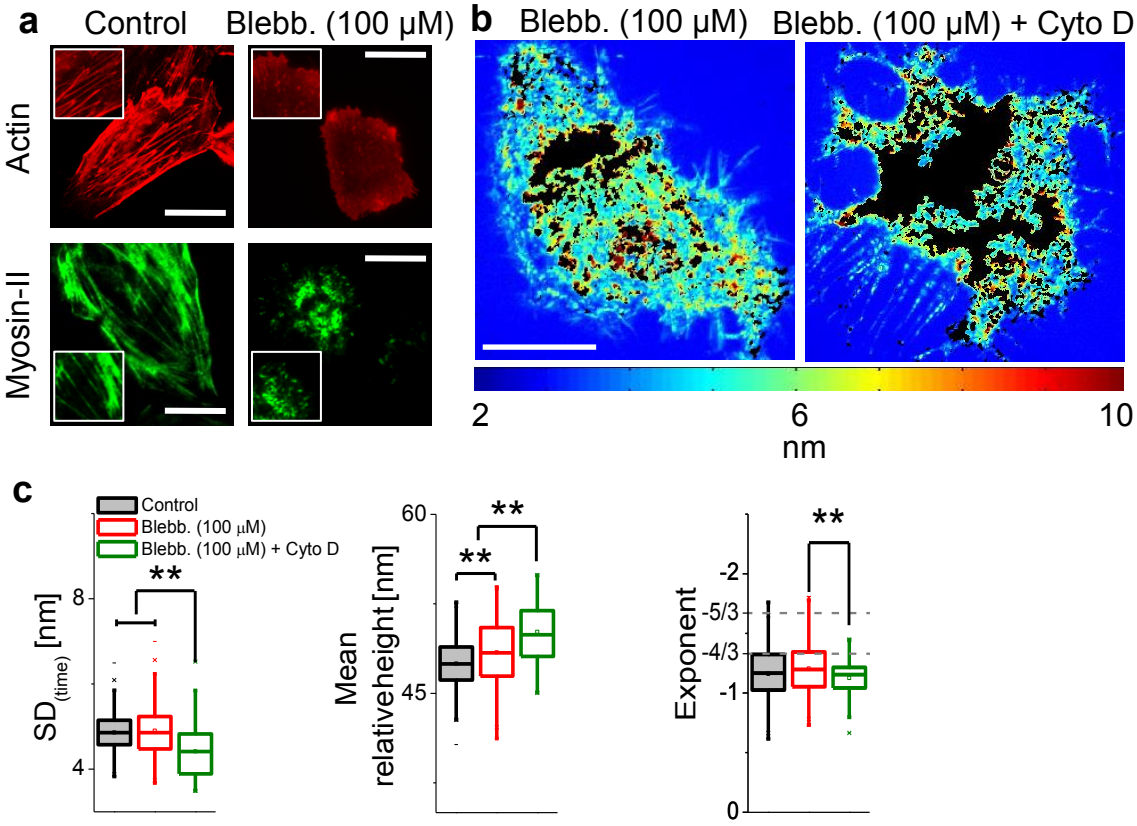

Figure S12. Detailed parameters towards the effect of polymerization on blocking Cyto D induced cortex clearance by pretreatment with Blebb. at a higher concentration.

(a) Representative epi-fluorescence images of actin (cells stained by Phalloidin-Rhodamine) and representative TIRF images of myosin II (cells transfected with pEGFP-mRLC1) in control and Blebb. (100 µM) treated HeLa cells. Scale bar: 10 µm. (b) Representative $SD_{(time)}$ maps (non-FBR regions blocked in black) of whole cells for Blebb. (100 µM) (left) and Blebb. (100 µM) + Cyto D treated (right) cells. Scale bar: 10 µm. (c) The parameters of temporal fluctuations ($SD_{(time)}$, Mean relative height and Exponent) in the different conditions (N = 10 each, $n_{control}$ = 165 FBRs, n_{Blebb} = 195 FBRs and $n_{Blebb+CD}$ = 72 FBRs). Asterisks indicate a significant difference (** $p < 0.001$, One-way ANOVA). See also **Tables S2 and S4**.

Figure S13

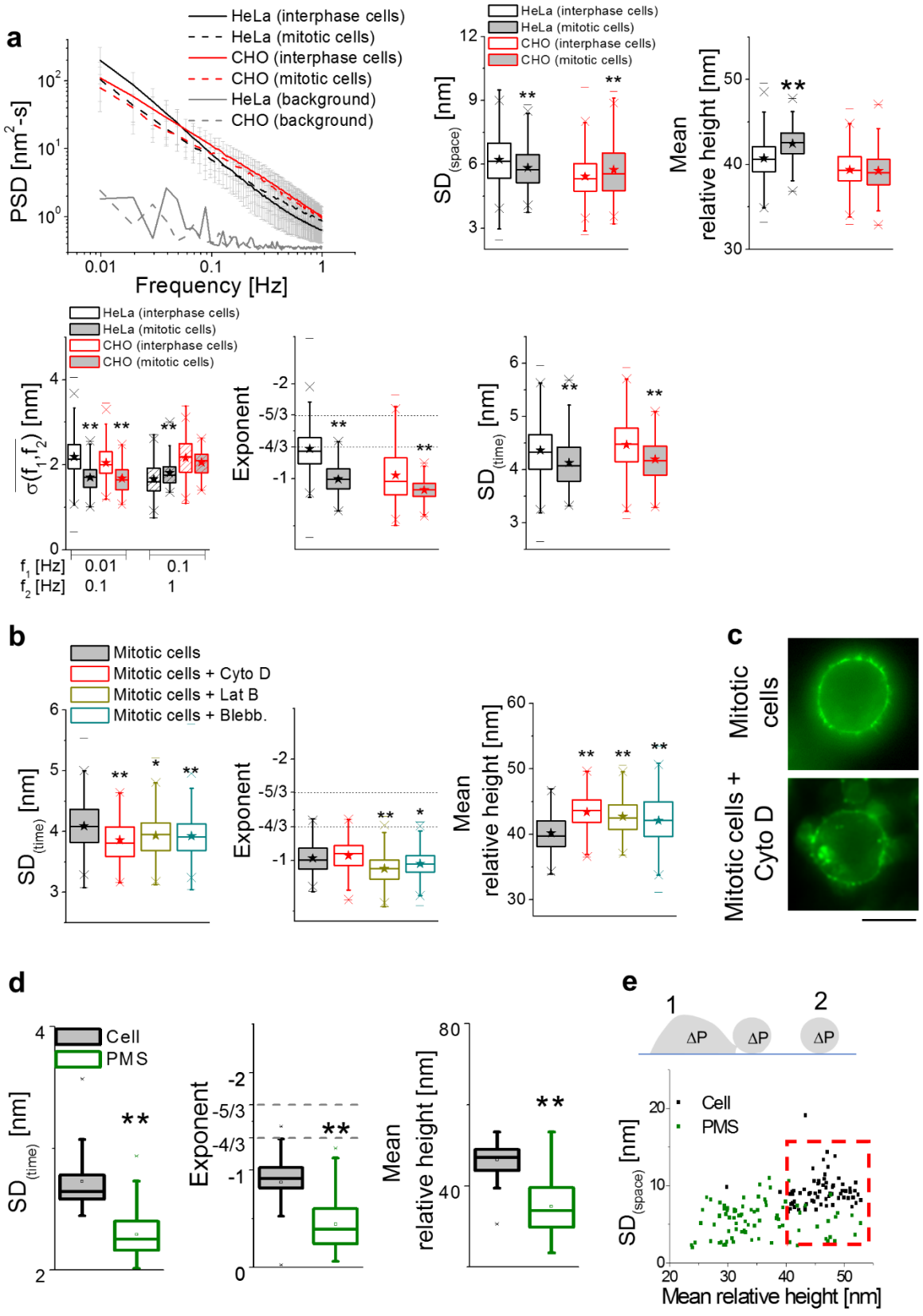
a
HeLa (interphase cells)
HeLa (mitotic cells)
CHO (interphase cells)
CHO (mitotic cells)
HeLa (background)
CHO (background)
PSD [nm²-s]
Frequency [Hz]
SD(space) [nm]
Mean relative height [nm]
σ(f1,f2) [nm]
Exponent
SD(time) [nm]
f1 [Hz] 0.01 0.1
f2 [Hz] 0.1 1
b
Mitotic cells
Mitotic cells + Cyto D
Mitotic cells + Lat B
Mitotic cells + Blebb.
c
Mitotic cells
Mitotic cells + Cyto D
d
Cell
PMS
e
ΔP
Cell
PMS
Mean relative height [nm]

Figure S13. Detailed parameters of membrane fluctuations during mitosis and in PMS.

(a) The averaged PSD of interphase (solid lines) and mitotic (dotted lines) HeLa (black) and CHO (red) cells with their backgrounds. Parameters of spatial undulations and temporal fluctuations of the interphase and mitotic cells in the two cell lines (N=10 cells each, $n_{interphase\ HeLa}$ = 328 FBRs, $n_{mitotic\ Hela}$ = 78 FBRs, $n_{interphase\ CHO}$ = 401 FBRs and $n_{mitotic\ CHO}$ = 60 FBRs). (b) The values of $SD_{(time)}$, Exponent and Mean relative height in mitotic cells, mitotic cells + Cyto D, mitotic cells + Lat B and mitotic cells + Blebb. (N = 15 cells each, $n_{mitotic\ cells}$ = 105 FBRs, $n_{,\ mitotic\ cells\ +\ Cyto\ D}$ = 85 FBRs, $n_{mitotic\ cells\ +\ Lat\ B}$ = 182 FBRs and $n_{mitotic\ cells\ +\ Blebb.}$ = 215 FBRs). (c) Representative images of mitotic cells stained with Alexa Flour 488 Phalloidin in the absence and presence of Cyto D. Scale bar: 10 µm. (d) The parameters of temporal fluctuations ($SD_{(time)}$, Exponent and Mean relative height) of cells and PMSs (N = 10 each, n_{cell} = 70 FBRs, n_{PMS} = 85 FBRs). ** mark a significant difference ($p<0.001$, One-way ANOVA). (e) Plot of $SD_{(space)}$ vs. mean relative height of cell derived PMS. Dotted region indicates cells and PMSs having the same relative height. Inset shows a schematic representation of a PMS pinched off but still adhered to the cell (1) and a cell free PMS (2) all having the same mean relative height and the same ΔP. See also **Tables S2 and S4**.

Figure S14

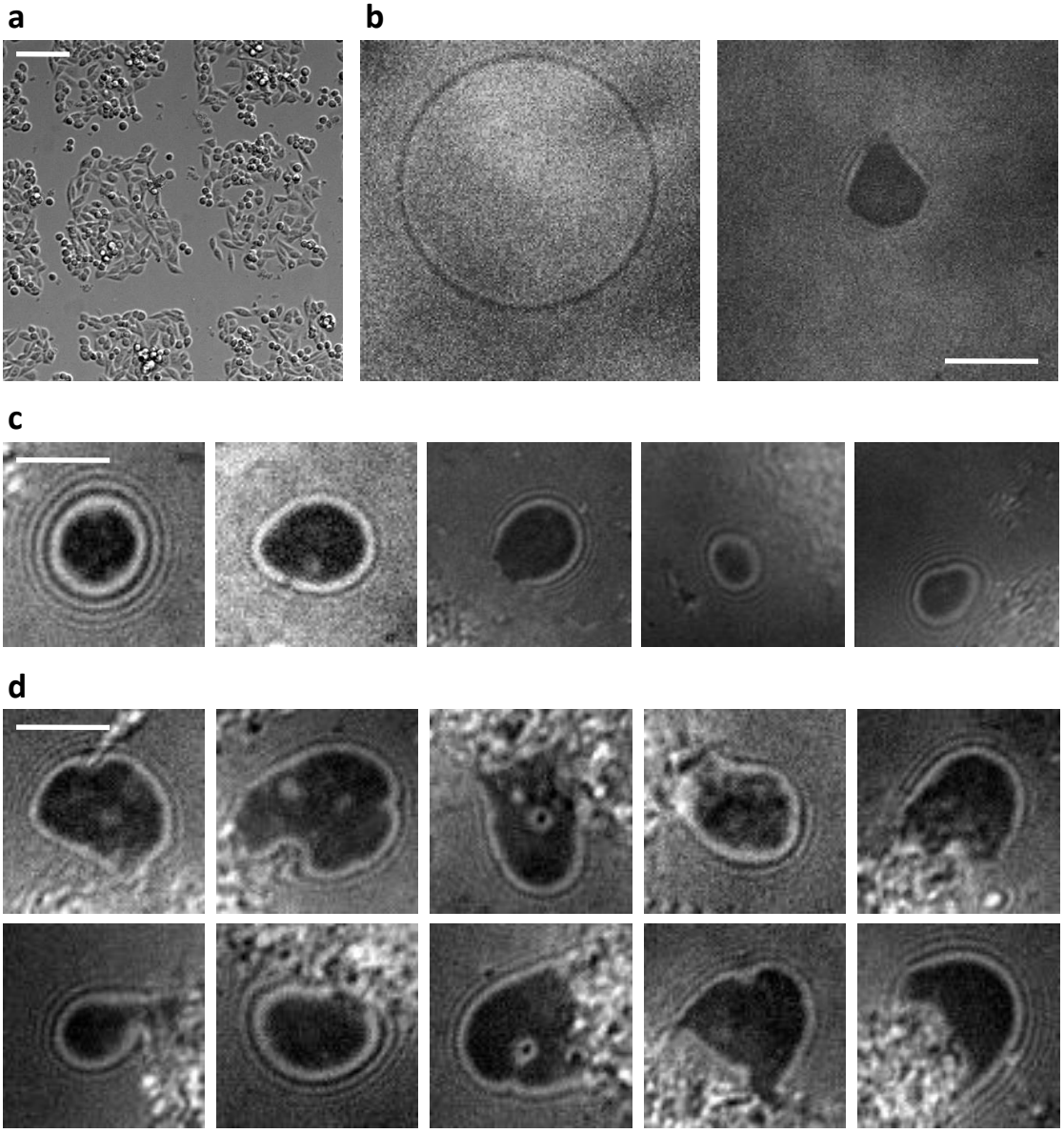

Figure S14. Types of PMSs.

(a) Micropatterned islands of CHO cells used for generating PMS. Scale bar: 30 μm. (b) Representative images of a PMS in DIC (left) and IRM (right) modes. Scale bar: 5 μm. (c) Representative IRM images of cell-free PMSs. Scale bar: 5 μm. (d) Representative IRM images of cell-attached PMSs. Scale bar: 5 μm.

Figure S15

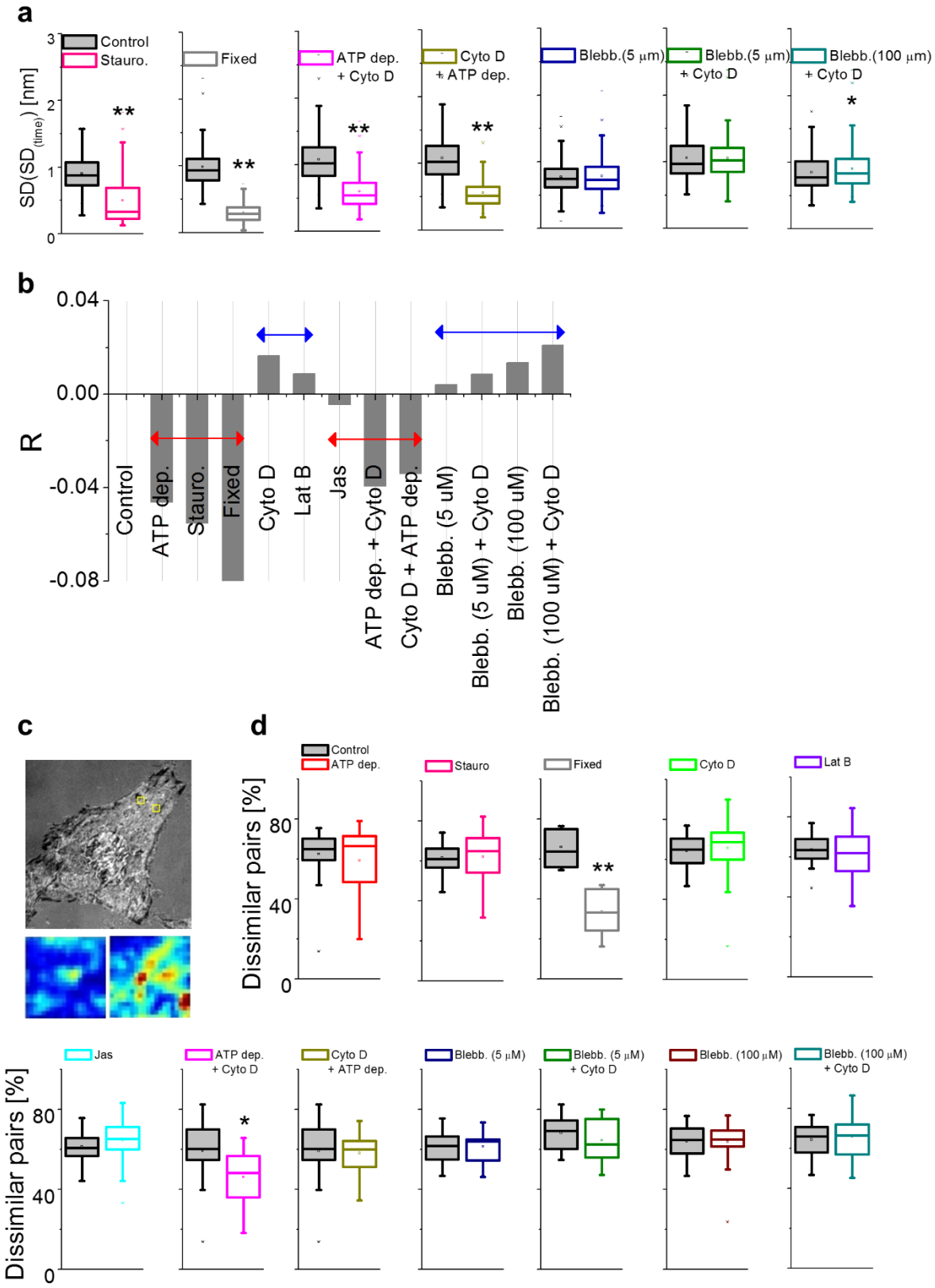
a
Control
Stauro.
Fixed
ATP dep.
+ Cyto D
Cyto D
+ ATP dep.
Blebb.(5 μm)
Blebb.(5 μm)
+ Cyto D
Blebb.(100 μm)
+ Cyto D
SD(SD(time)) [nm]
b
R
Control
ATP dep.
Stauro.
Fixed
Cyto D
Lat B
Jas
ATP dep. + Cyto D
Cyto D + ATP dep.
Blebb. (5 uM)
Blebb. (5 uM) + Cyto D
Blebb. (100 uM)
Blebb. (100 uM) + Cyto D
c
d
Dissimilar pairs [%]
Control
ATP dep.
Stauro
Fixed
Cyto D
Lat B
Jas
ATP dep.
+ Cyto D
Cyto D
+ ATP dep.
Blebb. (5 μM)
Blebb. (5 μM)
+ Cyto D
Blebb. (100 μM)
Blebb. (100 μM)
+ Cyto D

Figure S15. A measure of short and long length scale heterogeneities in cells.

(a) SD($SD_{(time)}$) for different conditions (N = 30 cells each). (b) Difference of ratio of SD($SD_{(time)}$) to Mean($SD_{(time)}$) of treated cells from that of control cell. $R = \left[\frac{SD(SD_{(time)})}{Mean(SD_{(time)})}\right]_{treated} - \left[\frac{SD(SD_{(time)})}{Mean(SD_{(time)})}\right]_{control}$. (c) Representative IRM image of a cell along with $SD_{(time)}$ maps of the two marked FBRs with the p-value measured to be 0.0009 by hypothesis testing (one-way ANOVA) of the $SD_{(time)}$ of the two. (d) Plots of the number of dissimilar pairs of FBRs (in %) between control and the treated sets. The parameters is calculated as $Dissimilar\ pairs = \frac{FBR\ pairs\ with\ SD_{(time)} having\ p<0.001}{Total\ no.\ of\ FBR\ pairs}$. * $p < 0.05$, ** $p < 0.001$, one-way ANOVA. See also **Tables S2 and S4**.

References

1. Limozin, L., and K. Sengupta. 2009. Quantitative reflection interference contrast microscopy (RICM) in soft matter and cell adhesion. ChemPhysChem. 10: 2752–2768.

2. Monzel, C., D. Schmidt, C. Kleusch, D. Kirchenbüchler, U. Seifert, A.-S. Smith, K. Sengupta, and R. Merkel. 2015. Measuring fast stochastic displacements of bio-membranes with dynamic optical displacement spectroscopy. Nat. Commun. 6: 8162.

3. Rodríguez-García, R., I.N. Ló Pez-Montero, M. Mell, G. Egea, N.S. Gov, and F. Monroy. 2015. Direct Cytoskeleton Forces Cause Membrane Softening in Red Blood Cells. Biophys. J. 108: 2794–2806.

4. Gov, N., A.G. Zilman, and S. Safran. 2003. Cytoskeleton confinement and tension of red blood cell membranes. Phys. Rev. Lett. 90: 228101.

5. Bicknese, S., N. Periasamy, S.B. Shohet, and A.S. Verkman. 1993. Cytoplasmic Viscosity Near the Cell Plasma Membrane: Measurement by Evanescent Field Frequency-Domain Microfluorimetry. Biophys. J. . 65: 1272–1282.

6. Kim, T., M.L. Gardel, and E. Munro. 2014. Determinants of Fluidlike Behavior and Effective Viscosity in Cross-Linked Actin Networks. Biophys. J. 106: 526–534.

7. Gov, N., and S.A. Safran. 2005. Red blood cell shape and fluctuations: Cytoskeleton confinement and ATP activity. J. Biol. Phys. 31: 453–464.

8. Betz, T., M. Lenz, J.-F. Joanny, and C.C. Sykes. 2009. ATP-dependent mechanics of red blood cells. PNAS. 106: 15320–15325.

9. Peukes, J., and T. Betz. 2014. Direct Measurement of the Cortical Tension during the Growth of Membrane Blebs. Biophys. J. 107: 1810–1820.

10. Lieber, A.D., S. Yehudai-Resheff, E.L. Barnhart, J.A. Theriot, and K. Keren. 2013. Membrane Tension in Rapidly Moving Cells Is Determined by Cytoskeletal Forces. Curr. Biol. 23: 1409–1417.

11. Fischer-Friedrich, E., A.A. Hyman, F. Jülicher, D.J. Müller, and J. Helenius. 2014. Quantification of surface tension and internal pressure generated by single mitotic cells. Sci. Rep. 6: 6213.